Soliton dynamics in an all-normal-dispersion photonic crystal fiber with frequency-dependent Kerr nonlinearity

Saili Zhao* and Xiaohong Sun
School of Information Engineering and Henan Key Laboratory of Laser and Opto-Electric Information Technology, Zhengzhou University, Zhengzhou 450001, China

(Received 7 July 2020; accepted 28 August 2020; published 16 September 2020)

We explore high-order soliton evolution in a composite all-normal dispersion photonic crystal fiber with frequency-dependent doping nonlinearity that can vary from positive to negative and vanish at a specific wavelength, named the zero-nonlinearity wavelength (ZNW). The change in frequency dependence of doping nonlinearity dramatically adjusts the position of the ZNW and the nonlinear strength acting on the supercontinuum spectral component. As the negative (positive) frequency dependence decreases (increases), one of two generated fundamental solitons via the combined action of negative nonlinearity and normal dispersion first has a gradually boosting soliton self-frequency shift (SSFS), and then a more suppressed SSFS, but is finally limited within an increasingly small spectral range while the other has a gradually decreasing SSFS toward the ZNW and radiates a broader and stronger phase-matched dispersive wave (DW) in the nonsolitonic region. Note that the collision between two fundamental solitons plays a significant role in regulating their temporal and spectral shift as well as energy redistribution. Furthermore, the numeric sign of the frequency dependence of doping nonlinearity provides another potential tool in controlling the spectral shift direction of fundamental solitons and DWs.

DOI: 10.1103/PhysRevA.102.033514

I. INTRODUCTION

In conventional fibers, a short optical pulse ejected by soliton fission can propagate as a fundamental soliton by balancing the interaction between anomalous group-velocity dispersion and self-phase modulation induced by positive Kerr nonlinearity [1,2]. In particular, photonic crystal fibers (PCFs) offer some additional advantages in the formation and propagation of fundamental solitons due to their design flexibilities in the dispersion and nonlinearity [2,3]. For example, it is possible to considerably regulate the Kerr nonlinear coefficient via utilizing different gases, liquids, and solids to fill the core of PCFs [4–6]. Such an adjustable nonlinearity provides the possibility to break the limitation that the formation of optical solitons requires anomalous dispersion since most optical fibers exhibit the positive nonlinearity at all wavelengths.

Recent studies have shown that the PCF doped with silver nanoparticles in its core can produce the effective doping nonlinearity that changes from positive to negative and vanishes at a specific wavelength called the zero-nonlinearity wavelength (ZNW) [7–9]. Such strong frequency dependence of doping nonlinearity and the existence of negative nonlinearity greatly change the general supercontinuum (SC) generation process, where the spectrum is dominated by the redshifted fundamental soliton and blueshifted dispersion waves (DWs) [2,10,11]. However, the existing studies of nonlinear dynamics in fibers with frequency-dependent Kerr nonlinearity mainly focused on the PCFs with one zero dispersion wavelength (ZDW), where the interval between ZDW and ZNW plays a crucial role in the evolution of an incident optical pulse [12,13]. Here we numerically study the propagation of a short optical pulse in an all-normal dispersion (ANDi) PCF with silver nanoparticles doped where the ZNW separates a solitonic region from a nonsolitonic one. By altering the frequency dependence of doping nonlinearity and the position of the ZNW with respect to the pump wavelength, some interesting phenomena are found. Particularly, temporal and spectral shifts of the generated fundamental soliton and dispersive wave (DW) as well as energy distribution of the overall SC spectrum vary significantly with the ZNW.

The paper is organized as follows. In Sec. II, we introduce the propagation equation used for studying the soliton dynamics in the fibers with frequency-dependent Kerr doping nonlinearity and adopt the normalized method to simulate the propagation model. In Sec. III, we show how the frequency dependence of effective doping nonlinearity affects the position of ZNW with respect to the input wavelength as well as the temporal and spectral evolution of incident short pulse propagation in the ANDi PCF. Section IV summarizes the main conclusions.

II. NUMERICAL MODEL FOR OPTICAL PULSE PROPAGATION IN A SILVER-DOPED ANDI PCF

We consider an ANDi PCF whose silica core is doped with silver nanoparticles as the propagation medium for incident optical pulse evolution. In this paper, it is assumed that the silver nanoparticles for adjusting the Kerr nonlinearity have no effect on Raman contribution and hence the Raman-induced

*iesallyzhao@zzu.edu.cn

spectral shift that appears to be nonphysical can be avoided during the pulse evolution [7,12]. According to this assumption for Kerr doping nonlinearity, a well-modified generalized nonlinear Schrödinger equation (GNLSE) is adopted to study the soliton dynamics in the ANDi PCF, taking the following form [1,12]:

$$\frac{\partial A}{\partial z} = -\frac{a}{2}A + \sum_{n=1}^{\infty} \frac{i^{n+1}\beta_n}{n!}\frac{\partial^n A}{\partial t^n} + i(1-f_R)\gamma_{\text{eff}}|A(z,t)|^2 A(z,t) + if_R\gamma A(z,t)\int_0^{\infty} h_R(t')|A(z,t-t')|^2 dt', \quad (1)$$

where $A(z,t)$ is a slowing varying time-domain pulse envelope, α is the linear loss constant, and β_n are the nth-order dispersion coefficients. γ_{eff} and γ are frequency-dependent nonlinear coefficients of the doped and undoped regions defined as $\gamma_{\text{eff}} = 2\pi\,\text{Re}(n_{2\text{eff}})/\lambda_0 A_{\text{eff}}$ and $\gamma(\omega) \approx \gamma_0 + \gamma_1(\omega-\omega_0)$, where $\gamma_0 = 2\pi n_2/\lambda_0 A_{\text{eff}}$ and $\gamma_1 \approx \gamma_0/\omega_0$ [7]. Even though the nonlinear refractive index is weakly frequency dependent for silica, it can be strongly frequency dependent for silver nanoparticles [13–15]. According to previous studies, the effective doping nonlinear coefficient γ_{eff} can be considerably adjusted by changing the filling factor, namely, the volume fraction of silver nanoparticle inclusions [7,12,16,17].

In order to simplify the complexity of simulation calculation, the adopted GNLSE need be normalized as follows [1,2]:

$$\frac{\partial u}{\partial \xi} = -\frac{i}{2}\text{sgn}(\beta_2)\frac{\partial^2 u}{\partial \tau^2} + \sum_{n=3}^{\infty} i^{n+1}\delta_n \frac{\partial^n u}{\partial \tau^n} + iN^2\text{sgn}(\gamma_{0\text{eff}}) \times (1-f_R)|u|^2 u + iN^2\sum_{m=1}^{\infty} i^m \mu_{m\text{eff}}(1-f_R)\frac{\partial^m}{\partial \tau^m}(|u|^2 u) + iN^2\left[\Gamma f_R|u|^2 u - \Gamma\tau_R u\frac{\partial|u|^2}{\partial\tau} + i\Gamma s f_R\frac{\partial}{\partial\tau}(|u|^2 u)\right], \quad (2)$$

where these parameters are normalized as $u = AP_0^{-1/2}$, $\delta_n = \beta_n/n!|\beta_2|T_0^{n-2}$, $L_D = T_0^2/|\beta_2|$, $\xi = z/L_D$, $\tau = (t - zv_g^{-1})/T_0 = T/T_0$, $L_{NL} = 1/|\gamma_{0\text{eff}}|P_0$, $N^2 = L_D/L_{\text{NL}}$, $\mu_{m\text{eff}} = \gamma_{m\text{eff}}/m!|\gamma_{0\text{eff}}|T_0^m$, $\Gamma = \gamma_0/|\gamma_{0\text{eff}}|$, $\tau_R = T_R/T_0$, and $s = 1/\omega_0 T_0$. Here, T_0, P_0, and v_g are initial pulse width, input peak power, and the group velocity of the pulse, respectively. $\gamma_{m\text{eff}}$ is the mth-order effective nonlinear coefficients obtained by a Taylor series expansion around the pulse center frequency ω_0 for the chosen filling factor, defined as $\gamma_{m\text{eff}} = (d^m\gamma_{\text{eff}}/d\omega^m)_{\omega=\omega_0}$. $\text{sgn}(\beta_2) = \pm 1$ implies a normal/anomalous dispersion region whereas $\text{sgn}(\gamma_{0\text{eff}}) = \pm 1$ indicates a positive/negative nonlinear medium.

In this paper, a hyperbolic secant pulse at a center wavelength of 1550 nm with $T_0 = 56.7$ fs pulse width is pumped into a 1.4-m-long ANDi PCF achieved by doping the silver nanoparticles in the core glass of the PCF used in Ref. [18]. At the pump wavelength, the dispersion and group-velocity curves of the ANDi PCF are shown in Fig. 1(a), whose dispersion coefficients are up to ninth order [18,19], as follows: $\beta_2 = 1.6735\times10^{-2}\,\text{ps}^{-2}/\text{m}$, $\beta_3 = -3.79\times10^{-5}\,\text{ps}^3/\text{m}$, $\beta_4 = 2.611\times10^{-7}\,\text{ps}^4/\text{m}$, $\beta_5 = -9.56\times10^{-10}\,\text{ps}^5/\text{m}$, $\beta_6 = 2.1365\times10^{-12}\,\text{ps}^6/\text{m}$,

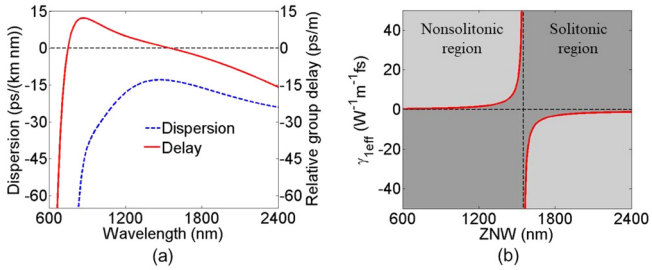

FIG. 1. (a) The curve of dispersion (blue dashed) and group delay (red solid) corresponding t the pump as a function of wavelength in the ANDi PCF. (b) $\gamma_{1\text{eff}}$ versus the ZNW in the ANDi PCF (solid red line). The vertical black dashed line shows the pump wavelength of 1550 nm. The light gray areas indicate the nonsolitonic region and the solitonic region is shown in dark gray.

$\beta_7 = -3.65\times10^{-15}\,\text{ps}^7/\text{m}$, $\beta_8 = -1.06\times10^{-17}\,\text{ps}^8/\text{m}$, $\beta_9 = 1.35\times10^{-19}\,\text{ps}^9/\text{m}$. The nonlinear coefficients of the undoped region at 1550 nm are $\gamma_0 = 0.0171\,\text{W}^{-1}\,\text{m}^{-1}$ and $\gamma_1 = 0.0141\,\text{W}^{-1}\,\text{m}^{-1}\,\text{fs}$. The frequency dependence of γ_{eff} in the doped region is included using $\gamma_{\text{eff}}(\omega) \approx \gamma_{0\text{eff}} + \gamma_{1\text{eff}}(\omega-\omega_0)$ with $\gamma_{0\text{eff}} = -0.5334\,\text{W}^{-1}\,\text{m}^{-1}$ and $\gamma_{1\text{eff}} = 12.36\,\text{W}^{-1}\,\text{m}^{-1}\,\text{fs}$ at the pump frequency, which can be accessed experimentally through the Z-scan technique [15]. The peak power of the input pulse is chosen to be $P_0 = 88$W such that the soliton order is $N = T_0\sqrt{|\gamma_{0\text{eff}}|P_0/|\beta_2|} \approx 3$. $\gamma_{1\text{eff}}$ representing the frequency dependence of doping nonlinearity greatly controls the position of ZNW and the slope of doping nonlinearity via its magnitude and sign. Since the filling factor used to adjust the doping nonlinearity is considered to be small, the doped ANDi PCF adopts the same Raman response function as the general silica optical fibers [12,13].

For general PCFs with positive nonlinearity at all wavelengths, the existence of ZDW gives rise to a series of fundamental solitons ejected into the solitonic region via soliton fission and the related dispersive waves (DWs) into the nonsolitonic region via satisfying the phase-matching condition [2,10], while for conventional ANDi PCFs, the lack of ZDW inhibits the formation of fundamental solitons [18–20]. It is worth noting that the above situation will change significantly due to the emergence of the ZNW in the ANDi PCF doped with silver nanoparticles. By changing the filling volume fraction of silver nanoparticles in the core of ANDi PCF, the frequency dependence of doping nonlinearity $\gamma_{1\text{eff}}$ can vary over a wide range even from positive to negative, resulting in the ZNW being located at different positions [12,13,17]. The relation between $\gamma_{1\text{eff}}$ and the ZNW is demonstrated in Fig. 1(b), where the vertical black line shows the pump wavelength of 1550 nm. As shown in Fig. 1(b), the ZNW separates the solitonic region from the whole wavelengths, which provides a prerequisite for the formation of fundamental solitons in the ANDi PCF since they can exist at the wavelengths for γ_{eff} and β_2 where have opposite signs.

III. NUMERICAL SIMULATION AND RESULTS

Let us first study the influence of $\gamma_{0\text{eff}}$ with positive and negative sign on the high-order soliton evolution when $\gamma_{1\text{eff}}$ is

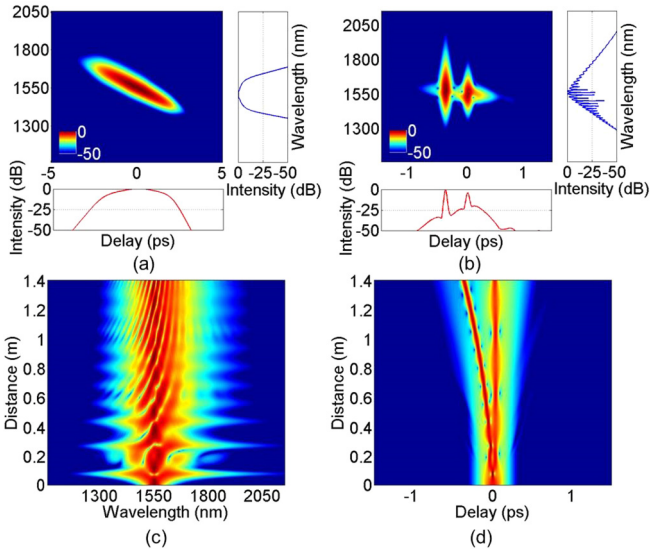

FIG. 2. When $\gamma_{1\text{eff}} = 0$: (a) output spectrogram of input pulse for $\gamma_{0\text{eff}} = 0.5334\,\text{W}^{-1}\,\text{m}^{-1}$ and (b) output spectrogram as well as the related (c) spectral and (d) temporal evolutions for $\gamma_{0\text{eff}} = -0.5334\,\text{W}^{-1}\,\text{m}^{-1}$.

not included. When $\gamma_{0\text{eff}}$ is positive, a high, flat SC spectrum is produced via the combined action of positive nonlinearity and normal group-velocity dispersion, as shown in Fig. 2(a). When $\gamma_{0\text{eff}}$ is negative, the entire wavelength band belongs to the solitonic region and there is no ZNW, resulting in the incident pulse beginning its evolution as a soliton. Due to the presence of negative doping nonlinearity, two distinct Raman solitons are excited via soliton fission, as shown in the output spectrogram of Fig. 2(b). In the absence of ZNW, the first-ejected fundamental soliton accelerates and shifts toward the red side due to the soliton self-frequency shift (SSFS) arising from intrapulse Raman scattering. Subsequently, the second-ejected Raman soliton is formed from the residual energy of the input high-order soliton and its center wavelength is approximately equal to the pump wavelength. It is noted that the second Raman soliton is in a semistable state, whose temporal profile is periodically compressed and broadened within the propagation distance. When the fiber structure remains the same, the second Raman soliton can also reach the steady state and then redshift to a longer wavelength via improving the peak power of the input pulse. Since this ANDi PCF provides a gradually increasing group velocity with increasing wavelength within the range of the generated SC spectrum, the Raman soliton generated at the longer wavelength has a higher intensity and a narrower temporal profile as well as a larger redshift in contrast with that at the shorter one, as shown in the spectral and temporal profiles of Figs. 2(c) and 2(d). Because one Raman soliton lies within the broad spectrum of another one, a series of interference fringes are formed in spectral evolution.

When we introduce a negative $\gamma_{1\text{eff}}$ and keep the other parameters the same, the evolution of high-order soliton pulse has changed dramatically. Figure 3 shows the temporal and spectral evolutions of input pulse in the ANDi PCFs with (a) $\gamma_{1\text{eff}} = -6.10\,\text{W}^{-1}\,\text{m}^{-1}$ fs (upper row), (b) $\gamma_{1\text{eff}} = -12.36\,\text{W}^{-1}\,\text{m}^{-1}$ fs (middle row), and (c) $\gamma_{1\text{eff}} = -18.35\,\text{W}^{-1}\,\text{m}^{-1}$ fs (lower row). The related output spectrograms as well as temporal and spectral profiles are shown in the right column for each case. For the three negative $\gamma_{1\text{eff}}$, the ZNWs of ANDi PCF are respectively located at 1670, 1607m and 1588 nm.

In the initial phase of pulse evolution, the combined effect of normal dispersion and negative nonlinearity gives rise to spectral broadening at a very fast rate. Due to the strong frequency dependence of doping nonlinearity, its strength acting on the whole frequency components is linearly varying and vanishes at the ZNW, further affecting the fission of a higher-order soliton into multiple fundamental solitons. As shown in Fig. 3, even though there are still two fundamental solitons ejected in the case with three different negative $\gamma_{1\text{eff}}$, their temporal and spectral shifts are greatly different from the situation of $\gamma_{1\text{eff}} = 0$. When $\gamma_{1\text{eff}} = -6.10\,\text{W}^{-1}\,\text{m}^{-1}$ fs, the fundamental soliton formed at the shorter wavelength decelerates and shifts toward the blue side while the other at the longer wavelength accelerates and shifts toward the red side. In contrast with the situation of $\gamma_{1\text{eff}} = -6.10\,\text{W}^{-1}\,\text{m}^{-1}$ fs the velocities of the two generated fundamental solitons decrease a little and their center wavelengths shift slightly toward the shorter wavelength when $\gamma_{1\text{eff}} = -12.36\,\text{W}^{-1}\,\text{m}^{-1}$ fs. However, the situation has changed dramatically in the case of $\gamma_{1\text{eff}} = -18.35\,\text{W}^{-1}\,\text{m}^{-1}$ fs, where the two generated fundamental solitons both accelerate and shift toward the red side but their redshift range is fairly narrow due to the position of the ZNW. Such phenomena result from the variation in magnitude of the frequency dependence of the doping nonlinearity changing the position of the ZNW and further affects the formation as well as the spectral shift trajectory of the fundamental soliton.

When zooming in on the temporal evolution at the front of the propagation distance, another intriguing phenomenon is found in Figs. 3(a) and 3(b), where the soliton formed at the shorter wavelength first accelerates a little and then slows down quickly after it collides with another soliton. As a further check, although the two solitons do not pass through each other, energy transfer and velocity change happen to them following the conservation of momentum and energy, which in turn leads to a new separation between them in the temporal and spectral domains. The phenomenon of energy transfer is characterized by the fundamental soliton at the shorter wavelength gaining a little energy from the other at the longer wavelength during soliton collision. It is well known that the Raman soliton can be transformed into a standard fundamental soliton propagating in fibers by adjusting its peak intensity or pulse width or the nonlinear strength it undergoes. Thus, the Raman soliton generated at the shorter wavelength first needs redshift to lower the strength of the negative doping nonlinearity it experiences to ensure that it can propagate as a fundamental soliton. Then the occurrence of a soliton collision brings about an increase in the peak power of the Raman soliton at the shorter wavelength but a decrease in its group velocity. In this case, the Raman soliton at the shorter wavelength has to blueshift and narrow its temporal width to maintain the state of the fundamental soliton. However, in Fig. 3(c), the fundamental soliton at the shorter wavelength has a lower peak intensity and a narrower temporal width

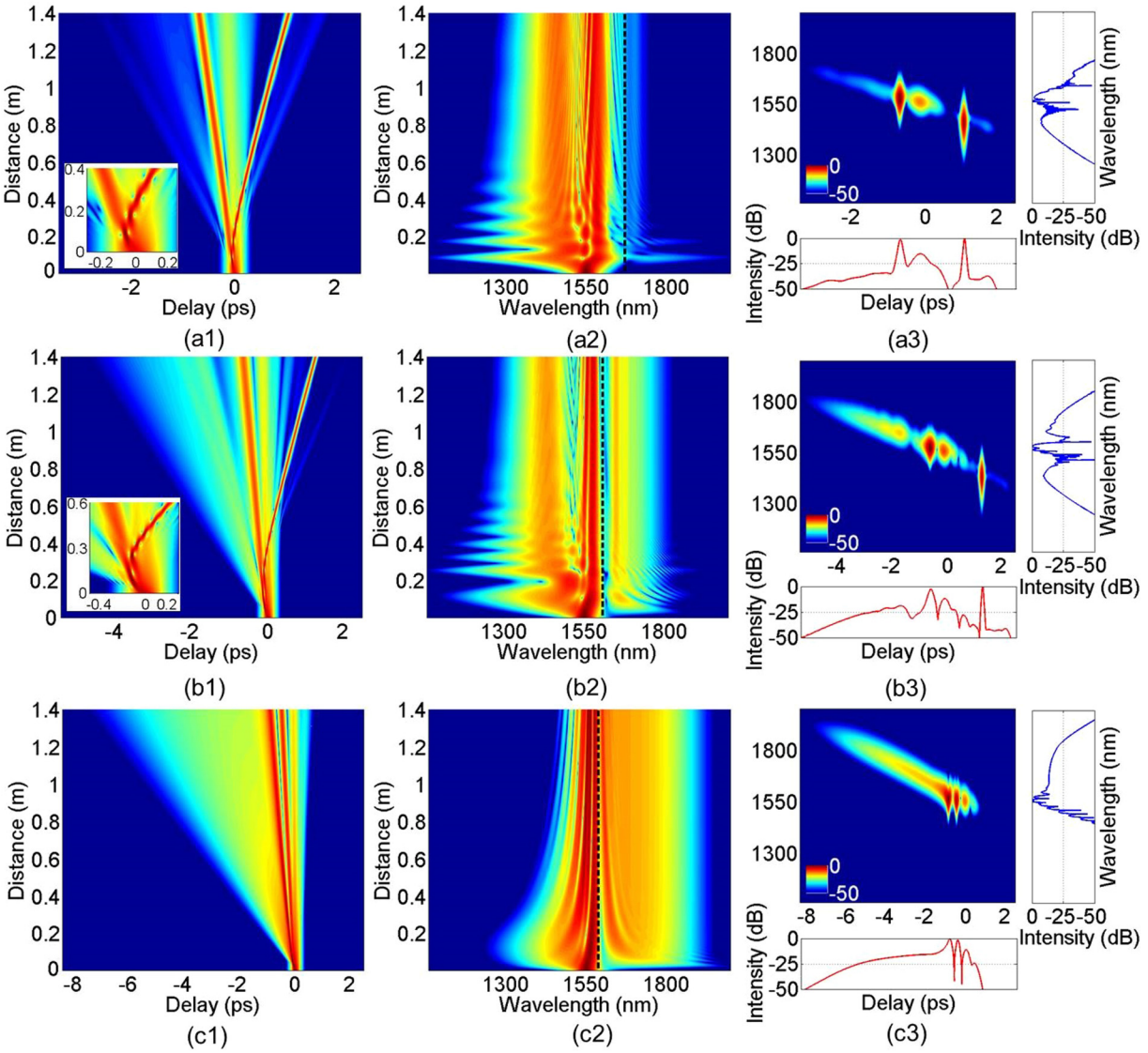

FIG. 3. (1) Temporal (left) and (2) spectral (middle) evolutions of input pulse for (a) $\gamma_{1\text{eff}} = -6.10\,\text{W}^{-1}\,\text{m}^{-1}$ fs (upper row), (b) $\gamma_{1\text{eff}} = -12.36\,\text{W}^{-1}\,\text{m}^{-1}$ fs (middle row), and (c) $\gamma_{1\text{eff}} = -18.35\,\text{W}^{-1}\,\text{m}^{-1}$ fs (lower row). The right column shows the output spectrogram as well as the temporal and spectral profiles for each case. The insets in (a1) and (b1) respectively show the amplification of the related parts. The black dashed lines in the middle column mark the ZNW.

in contrast with the other, resulting in the lack of a soliton collision and a continuous redshift acting on it.

As the negative $\gamma_{1\text{eff}}$ decreases, the ZNW of ANDi PCF gradually approaches the pump wavelength and the fundamental soliton located at the longer wavelength has a decreasing redshift within a limited transmission distance. As soon as the fundamental soliton reaches the vicinity of the ZNW, it radiates a part of its energy into the nonsolitonic region to form the DW under the condition of satisfying the phase matching. Subsequently, spectral recoil from the phase-matched DW suppresses a further redshift of the soliton. As expected, the decrease of negative $\gamma_{1\text{eff}}$ brings the ZNW much closer to the pump wavelength and further pushes more energy transferred into the nonsolitonic region to form the DWs. In addition, the total positive Kerr nonlinearity at the same wavelength of the nonsolitonic region increases rapidly with the decrease of negative $\gamma_{1\text{eff}}$, which contributes to the formed DW with an increasingly expanded spectrum. However, the ZNW in Fig. 3(a) is so far away that the soliton cannot move into the phase-matching spectral region and further suppress the formation of the DW. On the contrary, when the ZNW is much closer to the pump wavelength, both the amplification of the DW and the redshift of the generated fundamental solitons help their spectra merge together at the fiber output, as shown in Fig. 3(c).

The preceding scenario has shown how to excite a blueshifted fundamental soliton and amplify a red-shifted DW in the ANDi PCFs with negative $\gamma_{1\text{eff}}$. The phenomenon that we need to further explore is what happens to temporal and spectral evolutions of fundamental solitons and DWs if $\gamma_{1\text{eff}}$ is made positive. Here, the $\gamma_{1\text{eff}}$ term can be forcefully transferred from negative to positive via utilizing the nonlinear

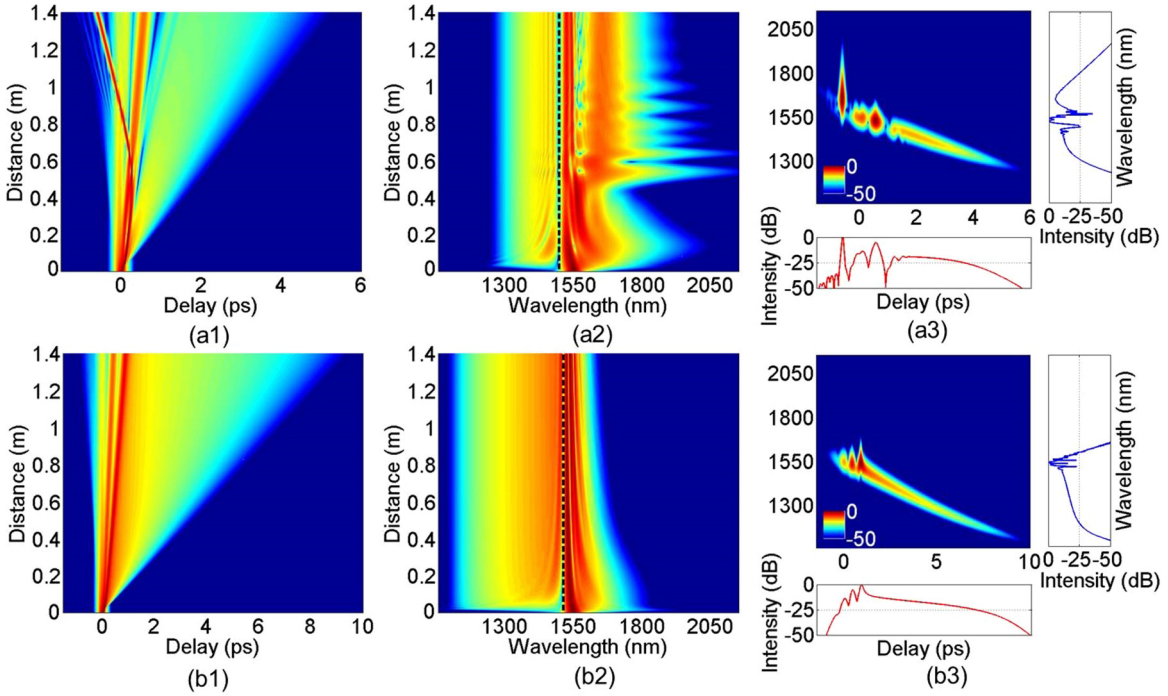

FIG. 4. (1) Temporal (left) and (2) spectral (middle) evolutions of the input pulse for (a) $\gamma_{1\text{eff}} = 12.36\,\text{W}^{-1}\,\text{m}^{-1}$ fs (upper row) and (b) $\gamma_{1\text{eff}} = 18.35\,\text{W}^{-1}\,\text{m}^{-1}$ fs (lower row). The right column shows the output spectrogram as well as the temporal and spectral profiles for each case. The black dashed lines in the middle column mark the ZNW.

metamaterial. In the case of positive $\gamma_{1\text{eff}}$, the ZNW is located at the wavelength shorter than the pump wavelength and separates the solitonic region (longer than the ZNW) from the nonsolitonic region (shorter than the ZNW).

When $\gamma_{1\text{eff}} = 12.36\,\text{W}^{-1}\,\text{m}^{-1}$ fs [Fig. 4(a)], the ZNW of the fiber is located at 1497 nm. In the initial stage of high-order soliton pulse evolution, two distinct fundamental solitons are ejected by soliton fission under the combined effect of normal dispersion and negative nonlinearity. The fundamental soliton formed at the shorter wavelength shifts toward the blue side and subsequently radiates the related phase-matched DW when it reaches the vicinity of the ZNW. Another soliton formed at the longer wavelength first blueshifts to reduce the strength of the negative doping nonlinearity acting on it so as to propagate as a fundamental soliton. However, the fundamental soliton located at the shorter wavelength goes through a little redshift during the blueshift of another soliton due to the mutual attraction between them, eventually leading to soliton collision in the temporal and spectral domains, as shown in Figs. 4(a1) and 4(a2). Then due to mutual repulsion, the two solitons separate again accompanied by the energy transfer between them, which causes the soliton located at the longer wavelength to increase the peak intensity and narrow the temporal width as well as start to redshift. Note that the two solitons do not pass through each other during the collision, which can also be concluded from the fact that the spectral overlap does not take place between them. When $\gamma_{1\text{eff}}$ increases to $18.35\,\text{W}^{-1}\,\text{m}^{-1}$ fs, it brings the ZNW of the PCF much closer to the pump wavelength and is located at 1514 nm. In this case, the two generated fundamental solitons are forced to blueshift and are restricted within a very narrow spectral range. In addition, a high-intensity broadband DW is formed in the nonsolitonic region resulting from the radiation of the fundamental soliton when the phase-matching condition is fulfilled. Therefore, the evolution of not only the fundamental soliton but also the DW is affected considerably by the magnitude and sign of the frequency dependence of the doping nonlinearity and the relative locations of the ZNW with respect to the input wavelength.

In order to more clearly understand the effect of $\gamma_{1\text{eff}}$ on the high-order soliton evolution in the ANDi PCF, we show the output pulse shapes and spectra under different $\gamma_{1\text{eff}}$, as shown below. From Fig. 5(b), the output position and intensity of fundamental solitons and DWs vary significantly with the ZNW. As the negative (positive) $\gamma_{1\text{eff}}$ decreases (increases), the output fundamental soliton formed at the shorter (longer)

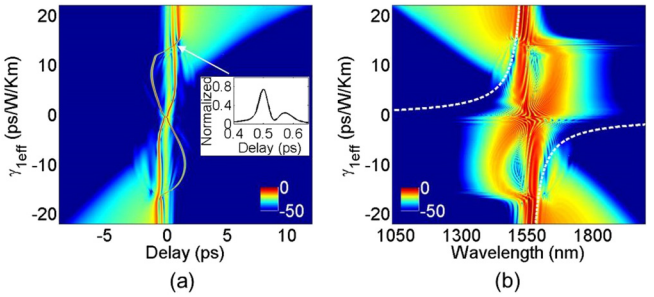

FIG. 5. Output (a) pulse shapes and (b) spectra versus $\gamma_{1\text{eff}}$ varying from -22 to $22\,\text{W}^{-1}\,\text{m}^{-1}$ fs. The inset in (a) shows the output temporal profile of two generated Raman solitons in the case of $\gamma_{1\text{eff}} = 13.9\,\text{W}^{-1}\,\text{m}^{-1}$ fs, indicating that the soliton collision happens at the end of PCF. The white dashed lines in (b) mark the ZNW varying with the $\gamma_{1\text{eff}}$.

wavelength first gradually blueshifts (redshifts), then in turn shifts toward the pump wavelength, and finally is limited to a narrow spectral range near the ZNW, while for the fundamental soliton formed at the longer (shorter) wavelength, it only redshifts (blueshifts) a little under the negative (positive) $\gamma_{1\mathrm{eff}}$. Remarkably, no matter how the temporal shift of two fundamental solitons changes with $\gamma_{1\mathrm{eff}}$, one of them at the longer wavelength has a smaller time delay in contrast with the other at the shorter wavelength depending on the group velocities of different spectral components in the ANDi PCF, as shown in Fig. 5(a). The inset in Fig. 5(a) shows the output temporal profile of two Raman solitons in the case of $\gamma_{1\mathrm{eff}} = 13.9\,\mathrm{W}^{-1}\,\mathrm{m}^{-1}$ fs, which indicates that the soliton collision happens at the end of the PCF and the energy is being transferred from the soliton at the shorter wavelength to that at the longer one. As the magnitude of negative (positive) $\gamma_{1\mathrm{eff}}$ increases, there is more energy transferred from the fundamental soliton into the nosolitonic region to form a DW with an increasingly expanded output spectrum and a gradually redshifting (blueshifting) center wavelength. Such phenomena result from the sign and magnitude of the frequency dependence of doping nonlinearity playing a considerable role in the center wavelength of the generated Raman soliton and further controlling the formation of DW via the phase-matching condition. In a word, the soliton dynamics becomes quite complex in the composite ANDi PCF which exhibits a strong frequency-dependent Kerr nonlinearity and brings a ZNW acting as a barrier between the soliton and the DW.

IV. CONCLUSIONS

In this work, we have numerically studied the temporal and spectral evolution of a high-order soliton pumped in the solitonic region of an ANDi PCF designed such that their effective doping nonlinear coefficient varies considerably with wavelength. More specifically, this paper mainly focused on how the magnitude and numeric sign of frequency dependence of doping nonlinearity affects the position of the ZNW as well as the formation and variation of fundamental solitons and the phase-matched DW. With the increase in the magnitude of frequency dependence, the ZNW gradually approaches the pump wavelength, hence helping more energy to be transferred from the fundamental soliton to the phase-matched DW. As a result, a smaller magnitude in the negative (positive) frequency dependence encourages a spectral blueshift (redshift) via the SSFS of a fundamental soliton while a larger one encourages a spectral redshift (blueshift) via the amplification of the DW. Therefore, the existence of the ZNW and the tunability of frequency dependence of doping nonlinearity provide a large degree of freedom in regulating the spectral shift and energy distribution of the fundamental soliton and DW in an ANDi PCF.

ACKNOWLEDGMENT

The work was supported by the Science and Technology Major Project, Henan Province (Grant No. 161100210200).

[1] G. P. Agrawal, *Nonlinear Fiber Optics*, 5th ed. (Academic Press, Oxford, 2013).
[2] J. M. Dudley, G. Genty, and S. Coen, Rev. Mod. Phys. **78**, 1135 (2006).
[3] C. Markos, J. C. Travers, A. Abdolvand, B. J. Eggleton, and O. Bang, Rev. Mod. Phys. **89**, 045003 (2017).
[4] M. F. Saleh, W. Chang, P. Hölzer, A. Nazarkin, J. C. Travers, N. Y. Joly, P. S. J. Russell, and F. Biancalana, Phys. Rev. Lett. **107**, 203902 (2011).
[5] S. Ertman, K. Rutkowska, and T. R. Woliński, J. Lightwave Technol. **37**, 2516 (2019).
[6] D. Poudereux, M. Caño-García, J. F. Algorri, B. García-Cámara, J. M. Sánchez-Pena, X. Quintana, M. A. Gedy, and J. M. Otón, Opt. Express **23**, 28935 (2015).
[7] S. Bose, R. Chattopadhyay, S. Roy, and S. K. Bhadra, J. Opt. Soc. Am. B **33**, 1014 (2016).
[8] R. Driben and J. Herrmann, Opt. Lett. **35**, 2529 (2010).
[9] R. Driben, A. Husakou, and J. Herrmann, Opt. Lett. **34**, 2132 (2009).
[10] I. Cristiani, R. Tediosi, L. Tartara, and V. Degiorgio, Opt. Express **12**, 124 (2004).
[11] D. V. Skryabin and A. V. Gorbach, Rev. Mod. Phys. **82**, 1287 (2010).
[12] S. Bose, A. Sahoo, R. Chattopadhyay, S. Roy, S. K. Bhadra, and G. P. Agrawal, Phys. Rev. A **94**, 043835 (2016).
[13] F. R. Arteaga-Sierra, A. Antikainen, and G. P. Agrawal, Phys. Rev. A **98**, 013830 (2018).
[14] R. W. Boyd, Z. Shi, and I. De Leon, Opt. Commun. **326**, 74 (2014).
[15] E. L. Falcão-Filho, C. B. de Araújo, A. Galembeck, M. M. Oliveira, and A. J. G. Zarbin, J. Opt. Soc. Am. B **22**, 2444 (2005).
[16] N. Zhavoronkov, R. Driben, B. A. Bregadiolli, M. Nalin, and B. A. Malomed, Europhys. Lett. **94**, 37011 (2011).
[17] V. S. Tiwari, A. Khetani, A. Momenpour, and H. Anis, IEEE J. Sel. Top. Quantum Electron. **20**, 7300608 (2014).
[18] I. A. Sukhoivanov, S. O. Iakushev, O. V. Shulika, E. Silvestre, and M. V. Andrés, J. Lightwave Technol. **35**, 3772 (2017).
[19] S. Zhao, H. Yang, Y. Xiao, and H. Hu, Europhys. Lett. **126**, 24002 (2019).
[20] C. Huang, M. Liao, W. Bi, X. Li, L. Hu, L. Zhang, L. Wang, G. Qin, T. Xue, D. Chen, and W. Gao, Photon. Res. **6**, 601 (2018).